J Ther Eng, Vol. 11, No. 3, pp. 685−702, May, 2025

Journal of Thermal Engineering
Web page info: https://jten.yildiz.edu.tr
DOI: 10.14744/thermal.0000939

Research Article

Numerical investigation of mixed convection in a square lid-driven cavity with influence of orientation and nanoparticle addition on heat transfer characteristics: Multi-objective optimization approach

T. Ravi Kumar REDDY[1,*], D.R. SRINIVASAN[2]

[1]*Department of Mechanical Engineering, JNTU Ananthapur, Andhra Pradesh, 515002, India*
[2]*Department of Mechanical Engineering, JNTU College of Engineering, Kalikiri, Andhra Pradesh, 517234, India*

ARTICLE INFO

Article history
Received: 21 March 2024
Revised: 24 June 2024
Accepted: 27 June 2024

Keywords:
Cavity; Dimensionless Number and RSM; Horizontal; Lid-driven; Vertical Blocks

ABSTRACT

Response surface methodology is employed to optimize the operating variables (i.e., Reynolds number (150 ≤ Re ≤ 2500), Grashof number (10^3 to 10^6) and Richardson number (0.01 ≤ Ri ≤ 12) with different orientations (horizontal and vertical) blocks with mixed convection heat transfer is analysed. Initially, numerical investigations are carried out on a lid-driven cavity with different orientations by employing a laminar mixed convection phenomenon. Optimized results are considered for defining the new models to reduce computational time and effort. Obtained optimized results are validated with numerical results (Nusselt number) and found to be in good agreement. The present work analysis is carried out on a rectangular cavity with different geometries inserted horizontally and vertically by varying the distance (0.2 ≤ W/L ≤ 0.8). As the distance between the blocks varied, the Nusselt number was affected. Also, it is observed that with higher Ri and Re, an enhanced Nu number is observed with vertical compared to horizontal models. In the case of vertical model, maximum Nu is observed at a W/L distance of 0.5 and Ri of 0.043; however, in case of horizontal models at a W/L distance of 0.2 and Ri of 0.043. Ultimately, novel relationships between the Nu number with other dimensionless parameters (Gr, Re) with different orientations (W/L) have been established, with the intention of potentially using them in engineering design.

Cite this article as: Reddy TRK, Srinivasan DR. Numerical investigation of mixed convection in a square lid-driven cavity with influence of orientation and nanoparticle addition on heat transfer characteristics: Multi-objective optimization approach. J Ther Eng 2025;11(3):685−702.

INTRODUCTION

In fluid thermodynamics, mixed convection refers to the combined action of natural and forced convection processes in heat transfer. This condition arises when both pressure and buoyancy forces simultaneously influence the fluid motion. The extent of each convection mechanism's contribution to heat transfer is primarily governed by factors such as flow characteristics, temperature gradients,

***Corresponding author.**
*E-mail address: ravikumarreddy.phd@gmail.com

This paper was recommended for publication in revised form by Editor-in-Chief Ahmet Selim Dalkılıç

geometry, and orientation. Additionally, fluid properties play a critical role; for example, the Grashof number increases with temperature in liquids but peaks at a specific point in gases. Mixed convection heat transfer problems are prominent in a range of essential engineering applications [1], including atmospheric boundary-layer flows, heat exchangers [2–5], solar collectors [6, 7], nuclear reactors, and the cooling of electronic equipment [8, 9]. In such systems, the configuration of internal components, such as circuit boards within a confined geometry can significantly affect the local temperature distribution and the efficiency of heat transfer. Thus, considerable interest lies in optimizing geometric configurations by modifying block spacing and operating parameters to enhance thermal performance.

The current work fits into this context, investigating convective heat transfer in a lid-driven cavity with various geometries inserted at different locations, where the upper plate moves at constant velocity. Several prior studies have examined laminar and turbulent lid-driven cavity flows using experimental and numerical approaches [10–13], aiming to improve the understanding of thermal characteristics under natural [14, 15], forced [14–18], and mixed convection regimes [14, 19], including the influence of different cavity shapes [19, 20].

Shah et al. [21] examined the impact of hybrid nanofluids in a trapezoidal cavity containing internal obstacles under varying Reynolds (Re), Richardson (Ri), and Lewis numbers. They reported that maximum heat transfer occurred near the moving lid and adjacent regions. Among the dimensionless numbers, the Lewis number had a dominant influence on isotherm distribution due to greater thermal diffusivity. Haq et al. [22] numerically explored a hexagonal cavity with an internal cylindrical body and found that variations in parameters such as Re, Ri, Hartmann number, and obstacle configuration significantly affected isotherms and flow structure. Xiong et al. [23] performed a numerical analysis of mixed convection in triangular cavities with varying obstacle shapes and found that increasing Ri enhanced Nusselt number (Nu), while higher Hartmann numbers diminished it. Yasin et al. [24] studied parallelogram enclosures under magnetic influence using the finite element method and noted that natural convection dominated at higher Ri values, whereas forced convection prevailed at lower Ri. Jiang et al. [25] simulated a 3D cubic cavity with porous media and hybrid nanofluids subjected to rotating cylinders and magnetic fields, identifying those key parameters like angular speed, Darcy number, and magnetic field direction strongly influenced heat transfer and entropy generation.

Khan et al. [26] analyzed hybrid nanofluid behavior in a cavity with square obstacles, showing that increased Re reduced kinetic energy while higher Grashof numbers boosted Nu due to enhanced buoyancy effects. Ali et al. [27] studied magneto-convection with nanoparticle dispersion and found that a 5% nanoparticle concentration yielded the highest heat transfer. Magnetic field strength was observed to influence both fluid motion and thermal performance. Yaseen et al. [28] demonstrated the benefits of flexible wall motion in enhancing Nu within an open lid-driven cavity. Xiao et al. [9] investigated solar-assisted mixed convection in a microalgae biogas reactor, reporting higher wall shear and reduced Nu at elevated volume concentrations. Alsabery et al. [29] assessed hybrid nanofluids in wavy cavities and noted that both obstacle placement and nanoparticle concentration critically affected thermal performance. To explore the influence of Ri, Re, and W/L ratio on Nu, a multi-objective response surface methodology (RSM) was used [30–34]. Selimefendigil et al. [34] employed fuzzy-based optimization to assess heat transfer in square enclosures, while Aminossadati et al. [35] applied ANFIS-based approaches to validate thermal performance predictions.

The above literature review concluded that the numerical analysis on mixed convection is not yet performed in a cavity with variation of positions of rectangular blocks. The application of magnetic field is still limited in triangular cavities with obstacles at center. The reference of literature review shows the working fluid is either the nano-fluids or air itself. The present work is on water filled cavity. The main objective of this work is to use numerical methods to examine the convection process in a cavity with a lid-driven motion, which has two rectangular blocks within. To study the heat transfer in mixed convection with the variation of Grashof number. To study the heat transfer in mixed convection with the variation of Reynolds number. Optimization of obtained numerical results by using multi-objective optimization tool (Response Surface Methodology Approach).

PROBLEM DESCRIPTION

Geometry, Boundary Conditions and Numerical Assumptions

A numerical investigation is conducted on a square cavity [36, -37] of length L on all sides with two rectangular blocks maintained at different locations, as shown in Figure 1. In this study, the bottom wall is maintained with a higher constant temperature, whereas the upper wall is moved with constant velocity in unidirectional with a constant cold temperature. Side walls are assumed to be adiabatic [38-41]. Two rectangular blocks are maintained with a height of 0.8 and a width of 0.05, respectively. The current study is centred on a lid-driven hollow containing two rectangular blocks positioned vertically and horizontally at varying distances, as seen in Figure 1. The obtained convective heat transfer coefficient from the simulation from the bottom wall towards [42-44] the upper wall as the cold temperature as reference temperature is used to calculate the local Nusselt number from the expression [27, 28, 43, 455-8]:

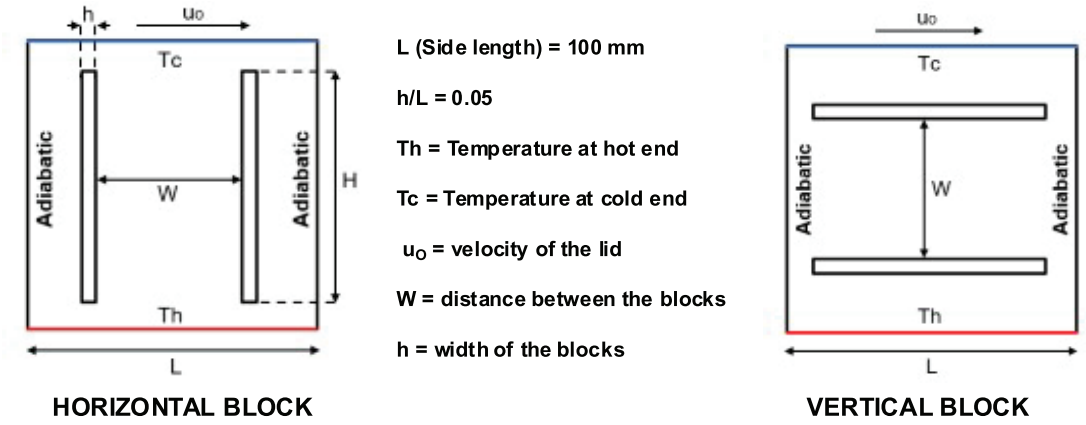

Figure 1. Computational model for the square cavity.

$$Nu(x) = -\left.\frac{\partial \theta}{\partial Y}\right|_{Y=0} \quad (1)\ [55]$$

$$Nu(x) = \int_0^1 Nu(x)dx \quad (2)\ [55]$$

In the present work analysis is carried out by considering laminar flow on a square cavity with different enclosures [35, 46-48]. The bottom part of the cavity is heated at a higher temperature and the top part is cooled and this temperature difference generates Rayleigh – Benard convection [49, 50]. The top part has a moving lid, which has a certain velocity. As both natural convection and mixed convection is happening, this problem is a mixed convection problem. In the present study, steady-state analysis is considered. The working fluid taken is air and the flow is considered to be incompressible [51]. The primary objective of this work is to conduct a numerical analysis of the mixed convection process in a lid-driven cavity containing two interior rectangular blocks. The working fluid is air and is believed to be incomp ressible. Simulations are carried out by using commercial software ANSYS Fluent to solve the governing equations (3-6) which are represented in a non-dimensional format. The linkage between velocity and pressure is established by the utilisation of the SIMPLE technique [38], while the attainment of a numerical solution's convergence is verified with a converging criterion of 10^{-5} for all the parameters [52].

$$\frac{\partial U}{\partial X} + \frac{\partial V}{\partial Y} = 0 \quad (3)$$

$$U\frac{\partial U}{\partial X} + V\frac{\partial U}{\partial Y} = -\frac{\partial P}{\partial X} + \frac{1}{\mathrm{Re}}\left(\frac{\partial^2 U}{\partial X^2} + \frac{\partial^2 U}{\partial Y^2}\right) \quad (4)$$

$$U\frac{\partial V}{\partial X} + V\frac{\partial V}{\partial Y} = -\frac{\partial P}{\partial X} + \frac{1}{\mathrm{Re}}\left(\frac{\partial^2 V}{\partial X^2} + \frac{\partial^2 V}{\partial Y^2}\right) + Ri.\theta \quad (5)$$

$$U\frac{\partial V}{\partial X} + V\frac{\partial V}{\partial Y} = \frac{1}{\mathrm{Re.Pr}}\left(\frac{\partial^2 \theta}{\partial X^2} + \frac{\partial^2 \theta}{\partial Y^2}\right) \quad (6)$$

The input parameters are Grashof Number and Reynolds Number. There are four different Grashof numbers and three different Reynolds numbers which are considered. A combination of each Grashof and Reynolds Number gives different cases. The output parameter is the Nusselt Number. Numerical investigation is carried out using commercial software ANSYS Fluent by employing finite volume method procedure. The heat transfer in 2-D surface of the square cavity with two blocks with different orientation is analysed.

Grid Sensitivity Analysis

Mesh creation refers to the process of creating a grid in two or three dimensions. The process involves partitioning complex geometries into constituent components. Meshing improves accuracy and reduces computational time. Meshing results in finite element analysis. Figure 2 illustrates the meshed domain for different orientations (vertical and horizontal). A very advanced mesh is used in close proximity to all solid walls, and a grid sensitivity test is conducted for both scenarios, as seen in Figure 3 [52].

Grid independence test is associated with the accuracy or even rationality of numerical results. The grid size is a crucial parameter in numerical analysis, since a smaller grid size will not provide sufficient precision, while a larger grid size would increase processing time. Consequently, the numerical model undergoes testing for grid independence and is compared to its experimental equivalents. For the present study grid independence test is done for different mesh sizes [53]. With vertical blocks in a cavity, mesh size with 21748 elements is considered. It is the optimal size of the mesh in order to get an optimized process to decrease the

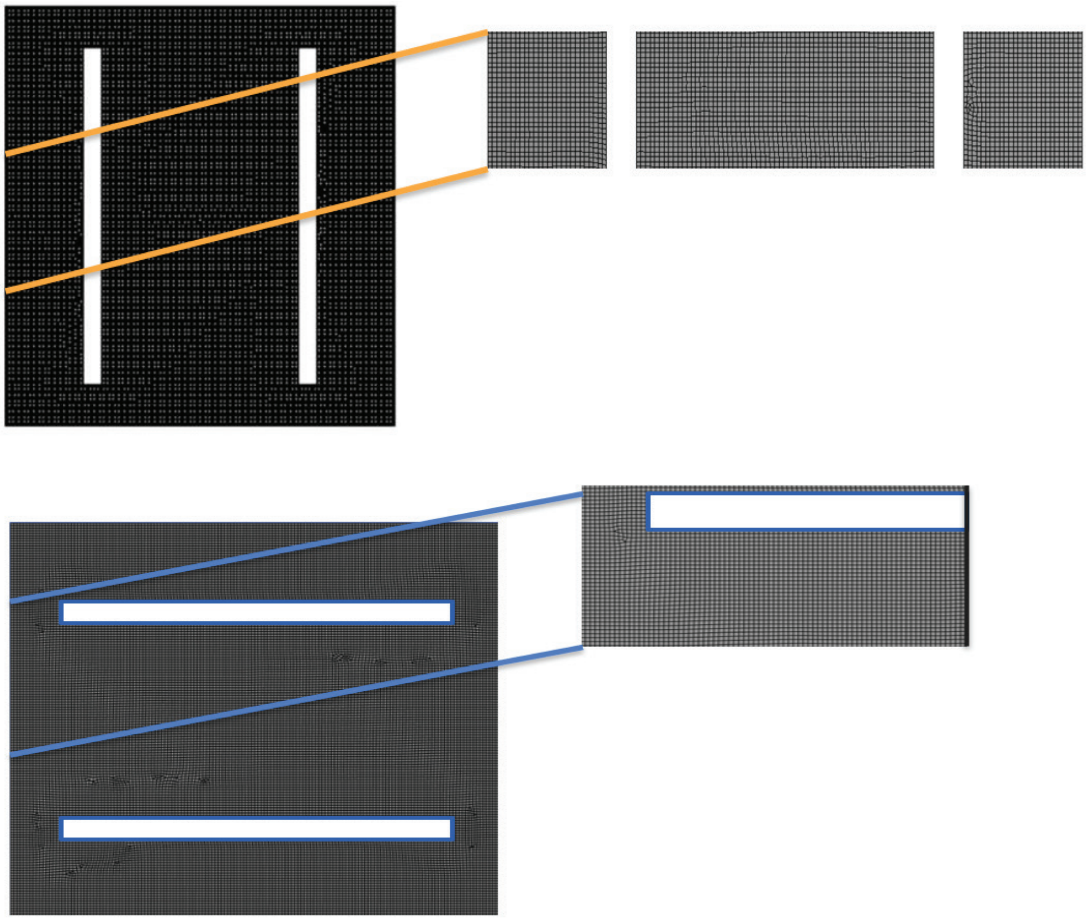

Figure 2. Mesh image for the square cavity with two different orientations of enclosures.

computational time. In the case of the square cavity with horizontal blocks, mesh size with 21812 elements is considered. It is observed that the deviation in average Nu between 25000 and 30000 elements is 0.16% in case of horizontal and 0.08% in case of vertical blocks respectively. Therefore, a total of 25000 components are selected for further examination, and it is noted that these results align well with the computational findings acquired from the existing literature.

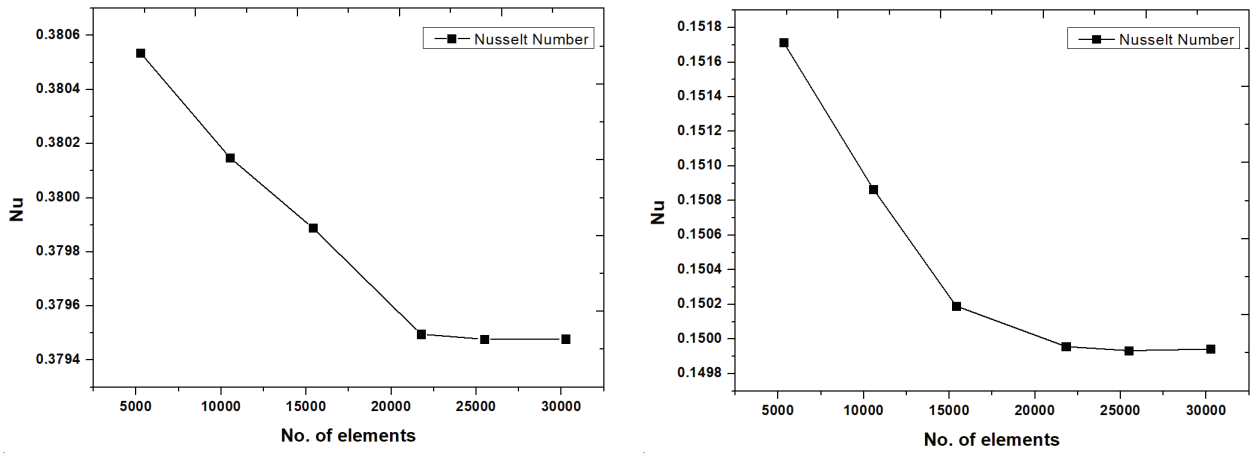

a) b)

Figure 3. Grid independent analysis a) Horizontal, b) Vertical orientations.

Table 1. Operating factors and their levels

Factors	Units	L-1	L-2	L-3
Gr	%	15000	30000	45000
Re	%	100	250	400
W/L	%	0.2	0.5	0.8

Table 2. L17 DOE with output responses

Input Control factors			Output Responses	
Gr	Re	W/L	$Nu_{Horizontal}$	$Nu_{Vertical}$
30000	250	0.5	0.012257	0.027684
45000	100	0.5	0.039881	0.037878
30000	250	0.5	0.012257	0.027684
30000	100	0.2	0.019613	0.065824
15000	250	0.8	0.006513	0.020383
45000	250	0.8	0.022033	0.07524
15000	400	0.5	0.007116	0.067853
45000	250	0.2	0.070816	0.18608
15000	100	0.5	0.00578	0.026369
30000	100	0.8	0.010705	0.04296
30000	250	0.5	0.012257	0.09887
30000	400	0.2	0.032366	0.135333
30000	400	0.8	0.013129	0.045477
45000	400	0.5	0.046193	0.250588
30000	250	0.5	0.012257	0.09887
30000	250	0.5	0.012257	0.09887
15000	250	0.2	0.008693	0.046215

Box-Behnken Response Surface Methodology Approach to find Optimal Parameters

The response surface technique employs many computational and mathematical methods to optimize and model the obtained results. Using the RSM reduces the number of tests conducted while simultaneously increasing accuracy and minimizing the use of time and energy. The RSM approach analyzes the stated parameters by establishing an appropriate relationship between the operational parameters. Before analyzing with Design Expert software, it is crucial to finalize the operating inputs and use an approximation function. The optimization of factors that impact the engine's performance is achieved using Response Surface Methodology (RSM). The experiments were conducted via the box-Behnken methodology, including 17 trials. For this study, three input parameters (Gr, Re, and W/L) are selected at equal intervals. Therefore, one output parameter, denoted as Nu, is set. To surpass the limitations of trial and operation setups, the engine input parameter ranges are conceptualized in an ideal manner. The experimental data were analyzed and interpreted using design expert software, and the results were included in a quadratic regression model.

The outputs are impacted by the input variables, which are then followed by the regression coefficient. The RSM model equations accurately forecast the best input parameters. The incorporation of CCD in the study facilitated the attainment of precise results. Table 1 presents the input variables for both orientations, whereas Table 2 presents the numerical design data.

RESULTS AND DISCUSSION

In the study of mixed convection of heat transfer, the CFD results for the two arrangements are being considered (Fig. 4). The content includes discussions on streamlines and isotherms, followed by the presentation of data for the Nu_{avg}. The Nusselt number is analysed as a function of the Ri and Re, with W/L serving as a parameter. The Reynolds and Richardson numbers under consideration include a

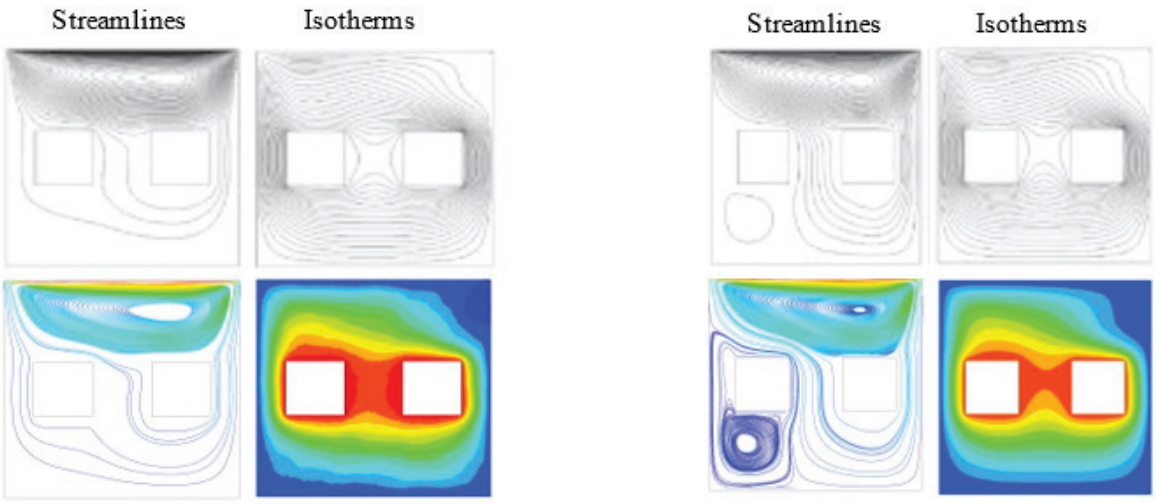

Figure 4. Validation of obtained results with Ri of 0.1 and 1.

range of (100 ≤ Re ≤ 500) and (0.00666 ≤ Ri ≤ 10), including both forced and natural convective-dominated regimes [52].

The technique is validated by comparing it to the numerical findings obtained in their examination of a lid-driven cavity with two internally heated square obstacles. The comparison of the streamlines and isotherms for the two validation cases, with Ri values of 0.1 and 1, demonstrates a full agreement between our results and those reported by Mandal et al. [52]. The model of validation is a square cavity with two square blocks in it. The W/L ratio in the validation case is 0.25. In this case the walls of obstacles are kept at high temperatures whereas the boundary walls of the outer square cavity are at low temperature. However, the upper lid is in motion in positive x direction. The validation cases taken with Reynolds number as 100 and varying Richardson number from 0.1 and 1. The obtained streamlines and isotherms are compared to our present work. The results show that the flow rate is reduced from the top to bottom. The streamlines form a vortex on the top whose size decreases as we move from left to right in case of Ri value 0.1. For Ri is equal to 1, another vortex besides the upper one is formed at the left corner.

Influence of Vertical Block Orientations on Thermal and Fluid Flow Structures

Figure 5 illustrates the isotherms and streamlines of square cavity with vertical orientations are enclosed with different spacings (W/L = 0.2, 0.5, 0.8), vary accordingly with Grashof number and Reynolds number. Generally, the streamlines can be observed by parting the square cavity into three regions. The left part is of the left rectangular block, the region in between the rectangular blocks, and the region right to the right rectangular block.

W/L = 0.2: In this case, when Gr = 10^5, three vortices are formed. When the Reynolds number is increased, the vortex formation is very clear. The pattern of the vortex intensifies with the increase in Grashof and Reynolds numbers. In the right channel, the size of the vortices is more than that of the left channel. It increases with the increase of the Grashof number. In the middle channel, there are not many formations of the vortices as there is less gap between the two obstacles. With the increase in the Reynolds number, the vortices can be seen at the middle chancel as well. The natural convective heat transfer dominates the forced convection at a higher Grashof number.

W/L = 0.5: One primary vortex can be seen in the case of a lower Reynolds number. As the Re is increased to 500, two vortices are formed. The main vortex is divided into two halves. It has occurred due to the interaction of opposite flow of fluids and is more significant at lower Reynolds and Grashof numbers. The secondary vortex is formed due to the detached flow of the fluid. One vortex is due to forced convection which is due to the moving lid at the top and the other one is due to the natural convection at the lower end of the block. As the Grashof number is increased, the natural convection dominates the forced convection and when the Reynolds number is increased, the forced convection dominates the natural convection.

W/L = 0.8: In the case of Gr = 10^5, two large vortices are formed. As the Reynolds number increases, the huge vortices almost completely occupy the central channel between the two blocks [52]. In this situation, the convective heat transfer resulting from the motion of the wall is more prominent than the natural heat transfer resulting from the wall›s high temperature [52]. This can be seen in the case of Gr = 10^5, Re = 500. The top vortex is larger in size when compared to the lower vortex. As the Re is increased in all the cases, the intensity of the top vortex is increased due to the forced convection. With the decrease in the Grashof number from 10^5 to 15000, the second vortex completely

W/L: 0.2			
	Re:100	**Re:250**	**Re:500**
Gr:105		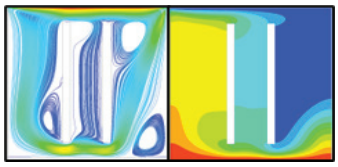	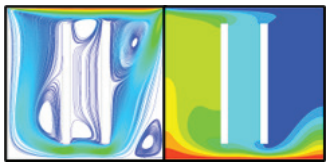
Gr:50000		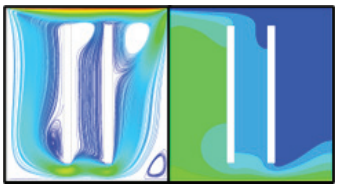	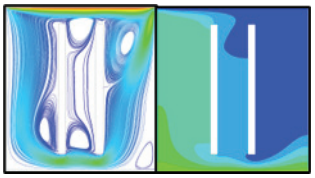
Gr:30000	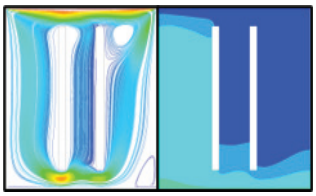		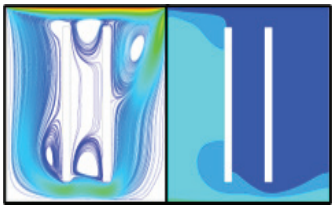
Gr:15000	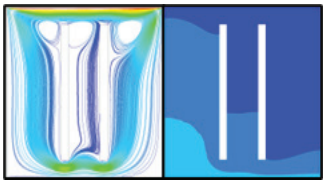		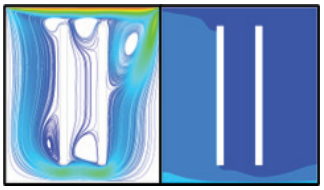

W/L: 0.5			
	Re:100	**Re:250**	**Re:500**
Gr:105	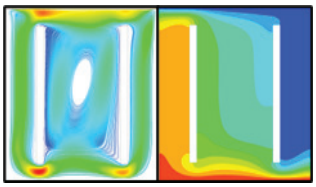	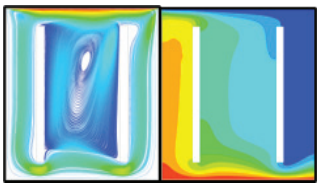	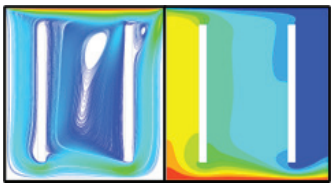
Gr:50000	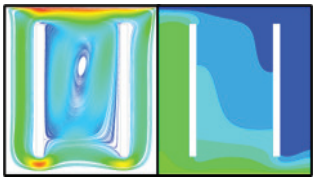	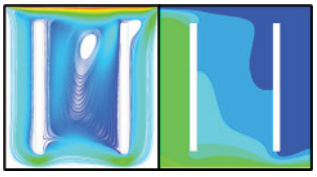	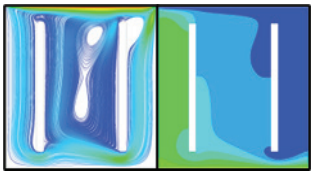
Gr:30000	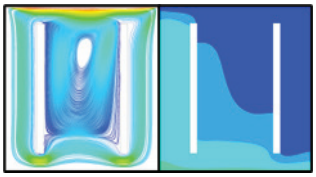	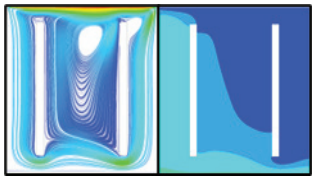	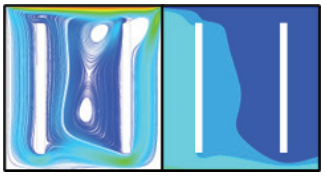
Gr:15000	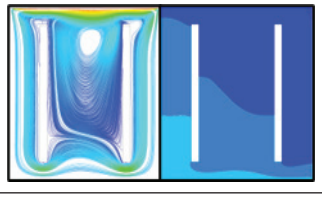	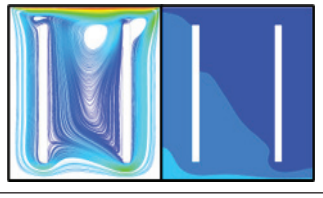	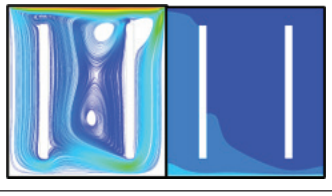

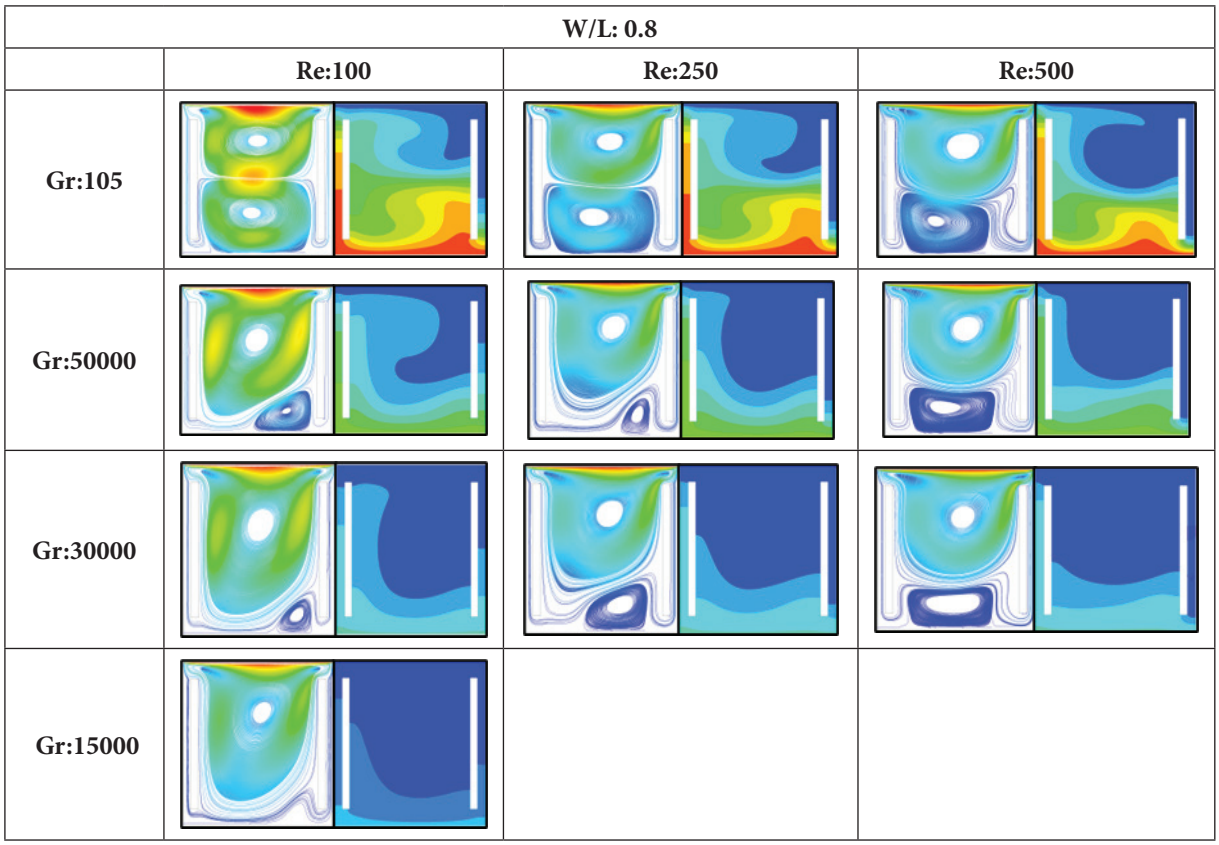

Figure 5. Thermal contours for vertical blocks.

disappears due to the decrease of the natural convection coefficient. Not much flow was observed near the left and right walls as there is very less space due to the obstacles. All the vortices are formed in between the walls. As the Reynolds number enhanced from 100 to 500, tiny vortices are formed along the bottom border of the block.

It is observed that the similar isothermal trends are observed for different orientations. The temperature at the bottom wall is high which is indicated by the isotherms which are predominantly denser at the bottom wall of the enclosure due to maximum temperature difference. The upper wall has a lid that is in motion, causing the cold flow to be generated by the movement of the lid. This flow is then transferred from the top to the bottom channel using a process of forced convection. The motion of the particles occurs due to the cold flow and the hot fluid which is present at the bottom is pushed into the middle which helps to achieve the greater Grashof number due to unbalanced cohesive forces. As the temperature rises, it signifies an escalation in the rate of heat transfer in close proximity to the lower surface of the hollow.

Influence of Horizontal Block Orientations on Thermal and Fluid Flow Structures

Figure 6 illustrates the isotherms and streamlines of square cavity with horizontal orientations are enclosed with different spacings (W/L = 0.2, 0.5, 0.8), vary accordingly with Grashof number and Reynolds number. Generally, the streamlines can be observed by parting the square cavity into three regions. The top part is on the upper rectangular block, the region in between the rectangular blocks and the region below the bottom rectangular block.

W/L = 0.2: For the W/L ratio 0.2, the exceptional cases occur at Gr = 10^5 and Re = 100 and Re = 250; Gr = 50000 and Re = 100. Other than these cases for all other values the vortices are formed in the top and bottom regions. For Gr value 10^5 and 50000 the vortices in the upper region change direction from left to right as the Reynolds number changes from 100 to 250. Whereas for all other values of the Grashof number the upper vortex is at the right side. The vortices at the bottom region are of different sizes. For all values of Grashof Number, the size of the vortex is large at Re = 250.

W/L = 0.5: Basically, in this case, the vortices are formed in the top and middle regions. The major difference between other cases with a W/L ratio of 0.2 or 0.8 is that there are two vortices formed in the upper region initially. As the Reynolds number increases the smaller vortex disappears dragging the larger vortex to the right.

W/L = 0.8: In this orientation, the vortices are formed in between the rectangular blocks. The two vortices vary the size but the trend changes at a Re value of 250. One of the vortices is formed at the edge of the lower horizontal rectangular block. And the second vortex is formed

W/L: 0.2			
	Re:100	**Re:250**	**Re:500**
Gr:105	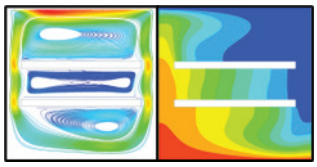	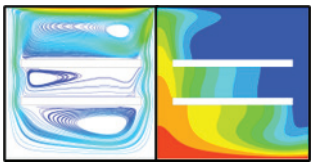	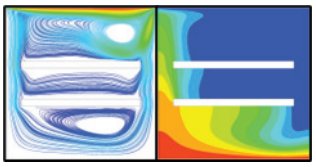
Gr:50000	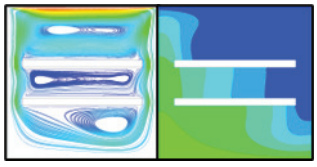	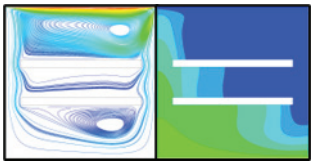	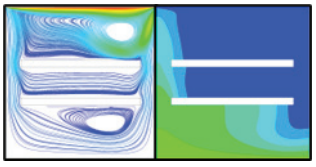
Gr:30000	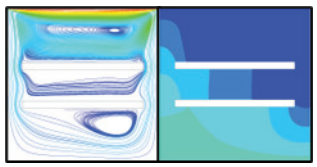	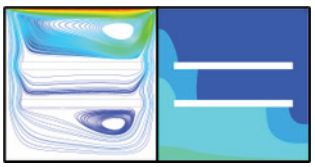	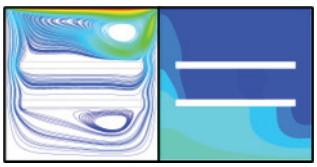
Gr:15000	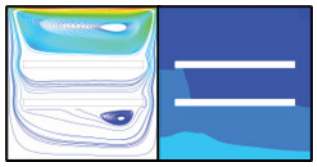	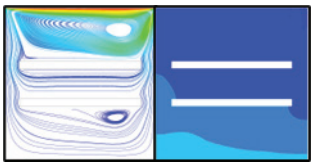	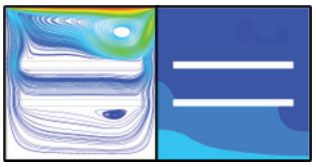

W/L: 0.5			
	Re:100	**Re:250**	**Re:500**
Gr:105	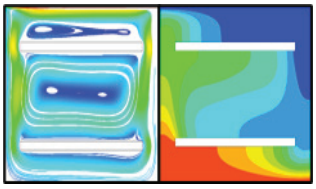	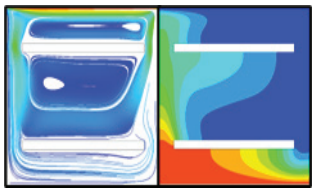	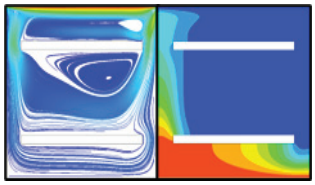
Gr:50000		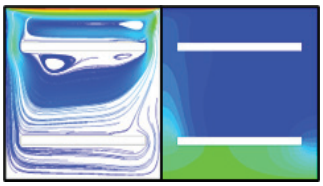	
Gr:30000		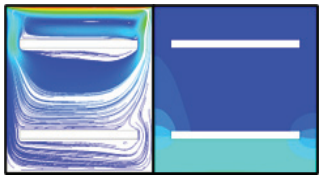	
Gr:15000			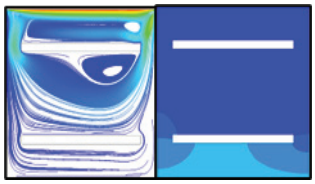

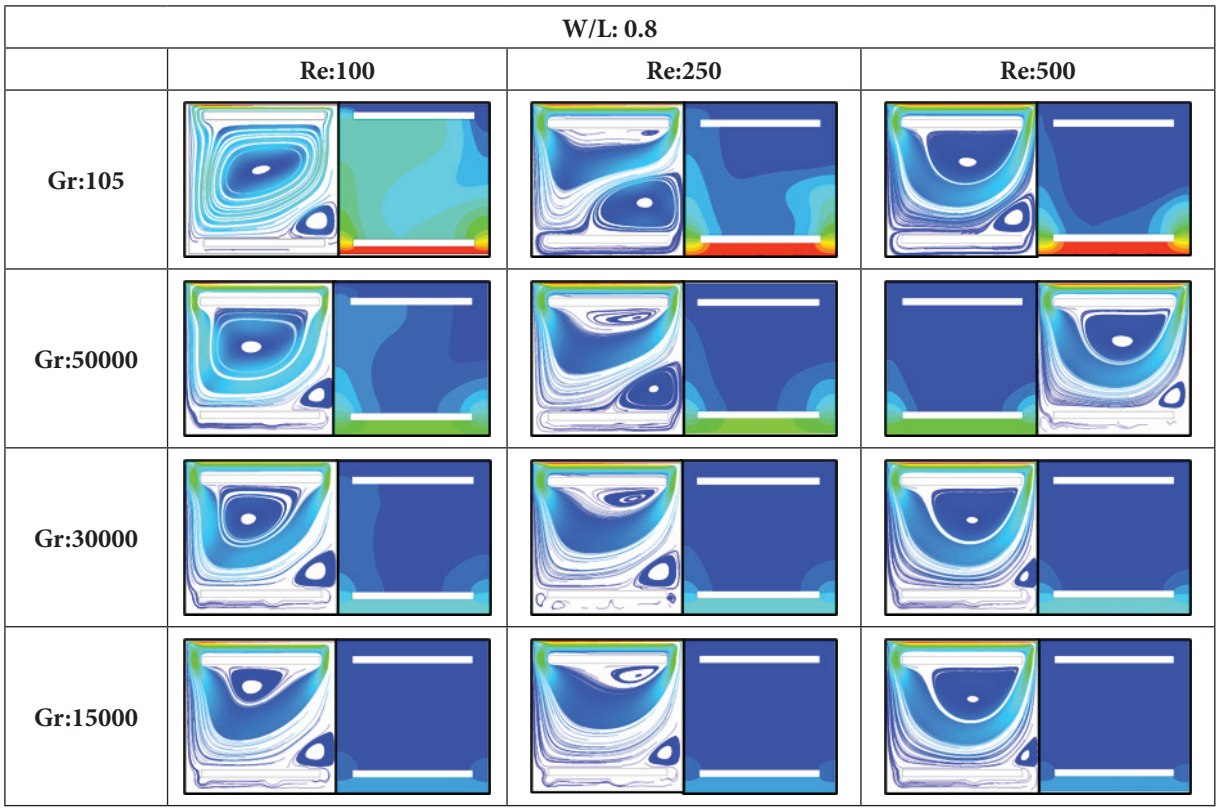

Figure 6. Thermal contours for horizontal blocks.

under the upper block. The presence of a second vortex in the upper middle area diminishes as the Reynolds number rises, but it remains prominent at a Reynolds number of 250. For the Grashof number 10^5 and 50000 the bottom vortex size increases and decreases with increased Reynolds number. For Gr = 30000 and Re = 15000, the bottom vortex size decreases with a rise in Re value.

In the isotherms as the temperature provided at the bottom wall is high the lower part is denser compared to the other regions and the flow of heat is in an upwards direction due to the orientation of the blocks. As the horizontal rectangular blocks serve as an obstacle to the actual flow of heat in the upper rightwards there is an occurrence of dynamic flow. The vigorous contours explain the mixed convection type of heat transfer.

Heat Transfer Rate Analysis

The Nusselt number here increases with both Grashof and Reynolds numbers. This is because natural convection enhances with an increase in Grashof number as temperature increases and forced convection enhances with a higher Re number as the lid velocity at the top increases. The results of the Nusselt numbers indicate that there is a minute reduction in the values. The Nusselt number values are high for Re = 500 for W/L equal to 0.2 and 0.8. And Nu value is high for Re = 250 for W/L = 0.2. Compared to all the orientation cases the highest Nu is in case of the closest arrangement of rectangular blocks that are for W/L = 0.2. The Figure 7 below illustrates the change of the Nu with the Ri for both the different orientations with spacing as a parameter. The variation trend can be seen from the plots of both the orientations. The statistics indicate that there is no coherent correlation between the Nusselt number and the Richardson number. The data suggest that there is no consistent relationship between the Nu and the Ri.

Ri can also be defined as the ratio of the Grashof number to the square of the Reynolds number [54, 55]. The Grashof number takes account of the natural convection and the Reynolds number takes account of the forced convection. It is observed that the lesser Ri number indicates the faster movement of upper lid or the lesser temperature of the bottom wall. The Figure 8 illustrates the influence of W/L on Nu with different Ri for both the orientation of the blocks. It can be seen that the variation in the case of vertical is more when compared to that of horizontal [56]. It is also observed that the maximum Nu of 0.478 is noted in vertical than that of horizontal (0.149) blocks. According to the results, it can be said that the Nusselt number is higher in the case of vertical in all the cases. However, drastic reduction is noted after 0.5 spacing in vertical orientation. But in the case of horizontal orientation, the difference is not very high and the plot is smooth [57]. From the above analysis it can be summarised that vertical blocks performed better compared with that of horizontal blocks. This is due to the lesser resistance enabling the colder fluid to move easily

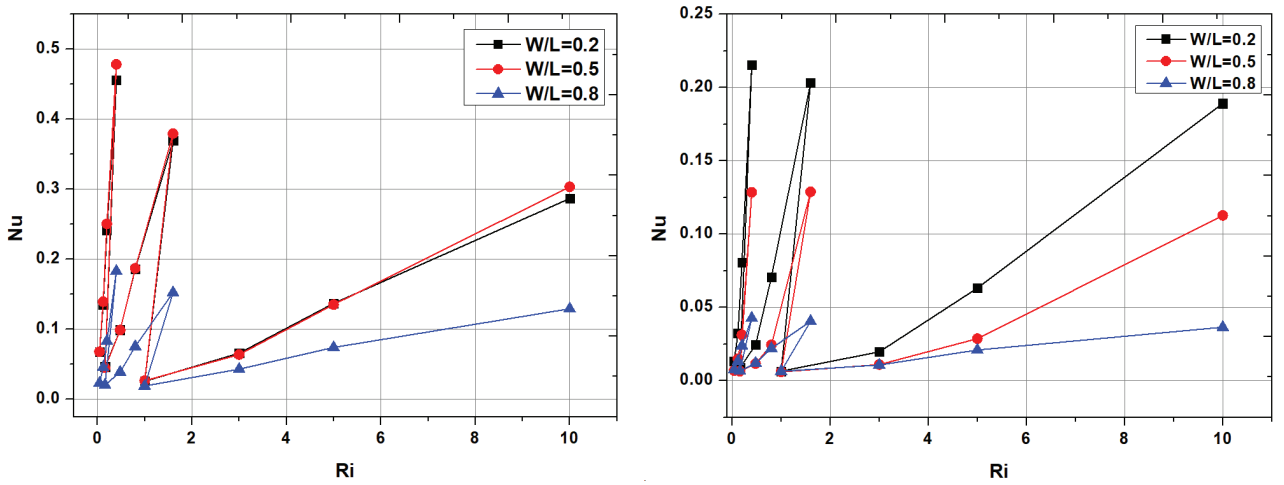

Figure 7. Influence of Ri on Nu with different W/L (Vertical and Horizontal blocks).

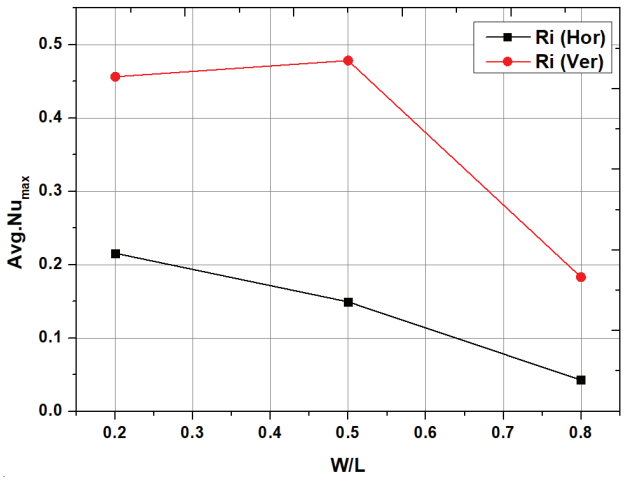

Figure 8. Influence of W/L on Nu with different Ri.

from the upper portion of the lid to the bottom portion which is maintained at constant higher temperature due to the spacing between the vertical blocks resulting in high temperature gradient and effective heat transfer rate (Nu). However, in case of the horizontal as the blocks are disrupting the flow resulting in obstruction gravitational forces making the fluid move towards side walls as the other path. Consequently, the circulation of cold air from the upper part is greatly diminished, resulting in just a little amount of air reaching the lower portion. The lower zone exhibits reduced convective currents and temperature gradients, resulting in a decline in the rate of heat transfer.

Mathematical Modelling Using MORSM

The 2nd order response surfaces corresponding to Nusselt number as a function of Grashof number, Reynolds number and W/L for both the horizontal and vertical blocks. To find the optimal parameters MORSM is employed initially to develop a regression model. In this method, the model obtained is assumed only for calculating the intercept as regressor. Achieving optimal results, a subset was created by sequentially inserting regressors into the model. It was noted that the response variable y, which was chosen as the initial variable to be employed, and the regressor had the most significant direct relationship with each other. The value X1 was presumed to be assigned to this regressor. During the analysis of regression, this particular regressor demonstrated the highest value for the F-statistic, indicating its significant relevance. If the adjustment is done to account for the impact of the first regressor-a_1 on the variable b, and the F-statistic exceeds a predefined F-value, then the second regressor selected for inclusion will exhibit the highest correlation with the variable b.

Once the adjustment is made to account for the influence of the first regressor-xl on the variable y, if the F-statistic exceeds a predetermined F-value, then the second regressor chosen for inclusion will have the strongest correlation with the variable y.

Analysis of Variance (ANOVA)

ANOVA assesses the influence of different experimental conditions on the results of the investigations. The ANOVA begins by evaluating the influence of each component and the likelihood of any potential outcomes. The second phase of ANOVA involves a detailed estimate of the significance of these influences. It was hypothesized that the experimental measurements follow a normal distribution for various experimental setups, with the F-test showing consistent variance (widely accepted). An analysis of variance (ANOVA) was conducted for all the response variables in this research. Tables 3 and 4 show the results of the ANOVA analysis for Nu in both the horizontal and vertical blocks. A mathematical equation was formulated for the purpose of conducting multiple regression analysis in order to develop predictive models.

Table 3. ANOVA model for Nu (horizontal and vertical)

	$Nu_{Horizontal}$		$Nu_{vertical}$	
Source	**F-Value**	**P-Value**	**F-Value**	**P-Value**
Model	160.22	< 0.0001	36.41	< 0.0001
Gr	985.83	< 0.0001	191.02	< 0.0001
Re	22.36	0.0021	36.78	0.0005
W/L	216.91	< 0.0001	56.94	0.0001
Gr*Re	0.3830	0.5556	0.7300	0.4212
Gr*W/L	89.01	< 0.0001	4.37	0.0749
Re*W/L	6.65	0.0365	6.73	0.0357
$(Gr)^2$	70.69	< 0.0001	0.4314	0.5323
$(Re)^2$	14.13	0.0071	0.0362	0.8545
$(W/L)^2$	25.00	0.0016	31.01	0.0008
Lack of fit	0.0002	3	0.0029	3

$Nu_{horizontal}$=0.1107+0.0619Gr+0.0093Re-0.0290W/L+0.0017(Gr*Re)-0.0263(Gr*W/L)-0.0072(Re*W/L)+0.0228$(Gr)^2$+0.0102$(Re)^2$+0.0136$(W/L)^2$

$Nu_{vertical}$=0.3144+0.0992Gr+0.0435Re-0.0541W/L+0.0087(Gr*Re)-0.0212(Gr*W/L)-0.0263(Re*W/L)+0.0065$(Gr)^2$+0.0019$(Re)^2$-0.0551$(W/L)^2$

The ANOVA results for the output parameters may be found in Tables 3, 4. The Design Expert software calculates regression coefficients, P-values, F-values, and R^2 values for statistical analysis. Through the computation of P-values and R^2 coefficient, one may assess the significance of anticipated models. P-values that are less than 0.05 are deemed significant, whereas smaller P-values and bigger F-values imply a greater relative significance for the corresponding term. Upon analysis and evaluation, it was found that the P-values for each projected model were less than 0.05, showing the significance of each model. R^2 may be used to compare experimental results with projected models. The R^2 values for the output variables, $Nu_{horizontal}$ and $Nu_{vertical}$, are 0.9952 and 0.9791, respectively. The R2 values for the projected models show a remarkable proximity to 1, indicating a significant degree of accuracy in comparison to the analytical outcomes [57].

Table 4. Model evaluation

Parameter	$Nu_{horizontal}$	$Nu_{vertical}$
Std.Dev	0.0056	0.0203
Mean	0.1326	0.2925
R^2	0.9952	0.9791
Adj R^2	0.9890	0.9522
Pred R^2	0.9227	0.8954

Influence of Operating Parameters on Nu

The predicted values are validated with the actual values for two different orientations are illustrated in the Figure 9. The R^2 values for the output variables $Nu_{horizontal}$ and $Nu_{vertical}$ are 0.96 and 0.94, respectively. The R^2 values for the projected models show a remarkable proximity to 1, indicating a significant degree of accuracy compared to the analytical outcomes. It has been noted that the effectiveness of the constructed prediction model is better when the values of comparative analysis and R^2 are low. The influence of operating parameters (Gr, Re and W/L) on Nu are determined by developing 2D plots. The pattern of the vortex intensifies with the increase in Grashof and Reynolds numbers. In the right channel, the size of the vortices is more than that of the left channel. It increases with the increase of the Grashof number. In the middle channel, there are not many formations of the vortices as there is less gap between the two obstacles. With the increase in the Reynolds number, the vortices can be seen at the middle chancel as well. The natural convective heat transfer dominates the forced convection at a higher Grashof number [58].

Optimization and Validation

Following the development of a predictive model, the optimization method was used to identify the optimal input parameters. In MORSM, the desirability technique was used to ascertain the optimal operating parameters. In this investigation, the Nu parameters were set to their maximum levels [58]. The desired degree of attractiveness is when the output and ideal operating conditions are reached [59, 60]. Figure 10 illustrates the desirable parameters for Nu horizontal and vertical blocks. The optimal values in case of $Nu_{horizontal}$ are at Gr (27888.1), Re (400) and W/L (0.2) is observed. The optimal values in case of $Nu_{vertical}$ are at Gr (44753), Re (394.89) and W/L (0.298) is observed.

A confirmation test uses the optimal conditions identified via desirability analysis. The confirmation outcomes for Nu. The study›s findings align with the optimal conditions, and the margin of error in the confirmation tests is within an acceptable range [61].

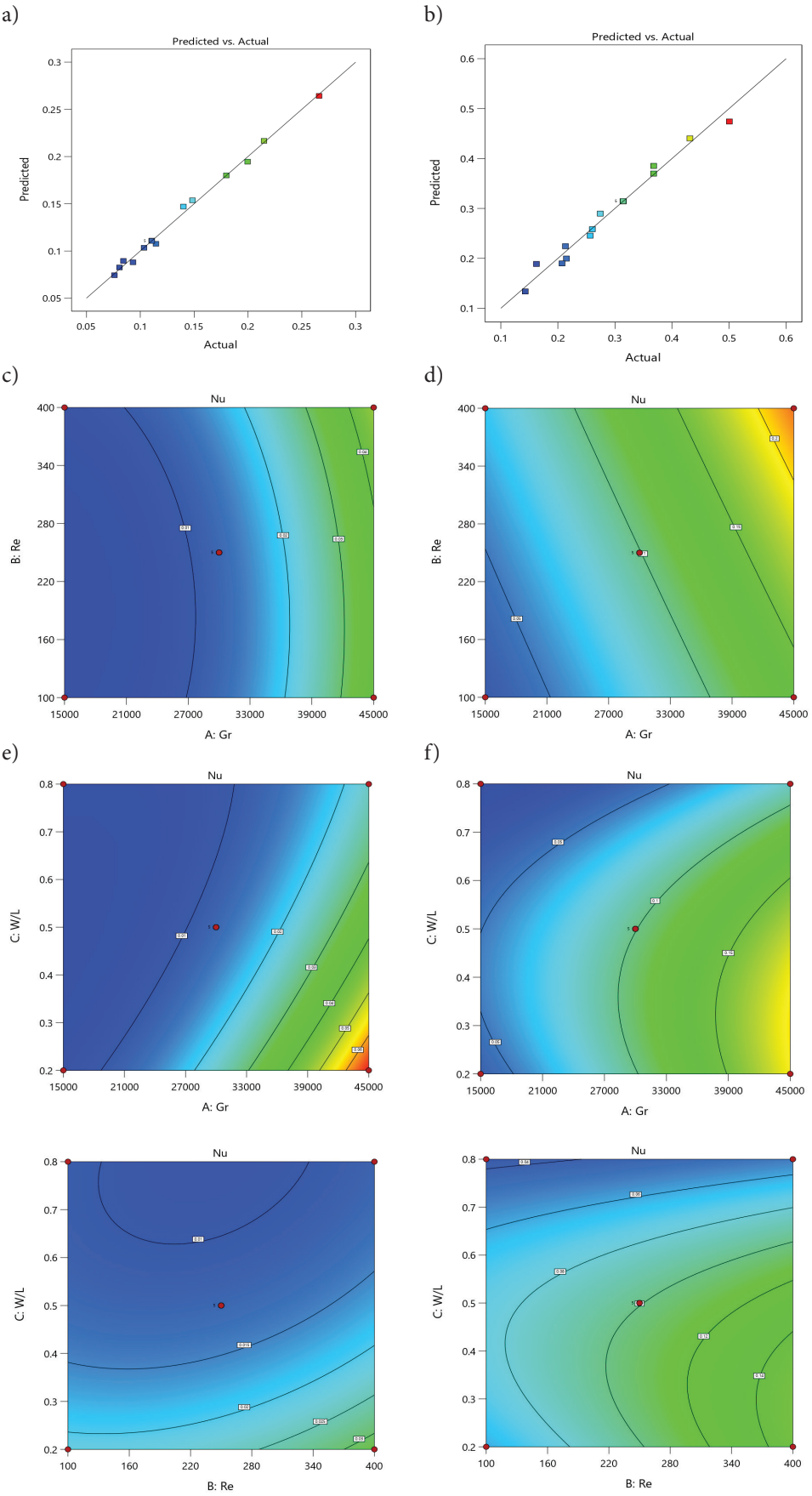

Figure 9. 2 D contours for different operating parameters.

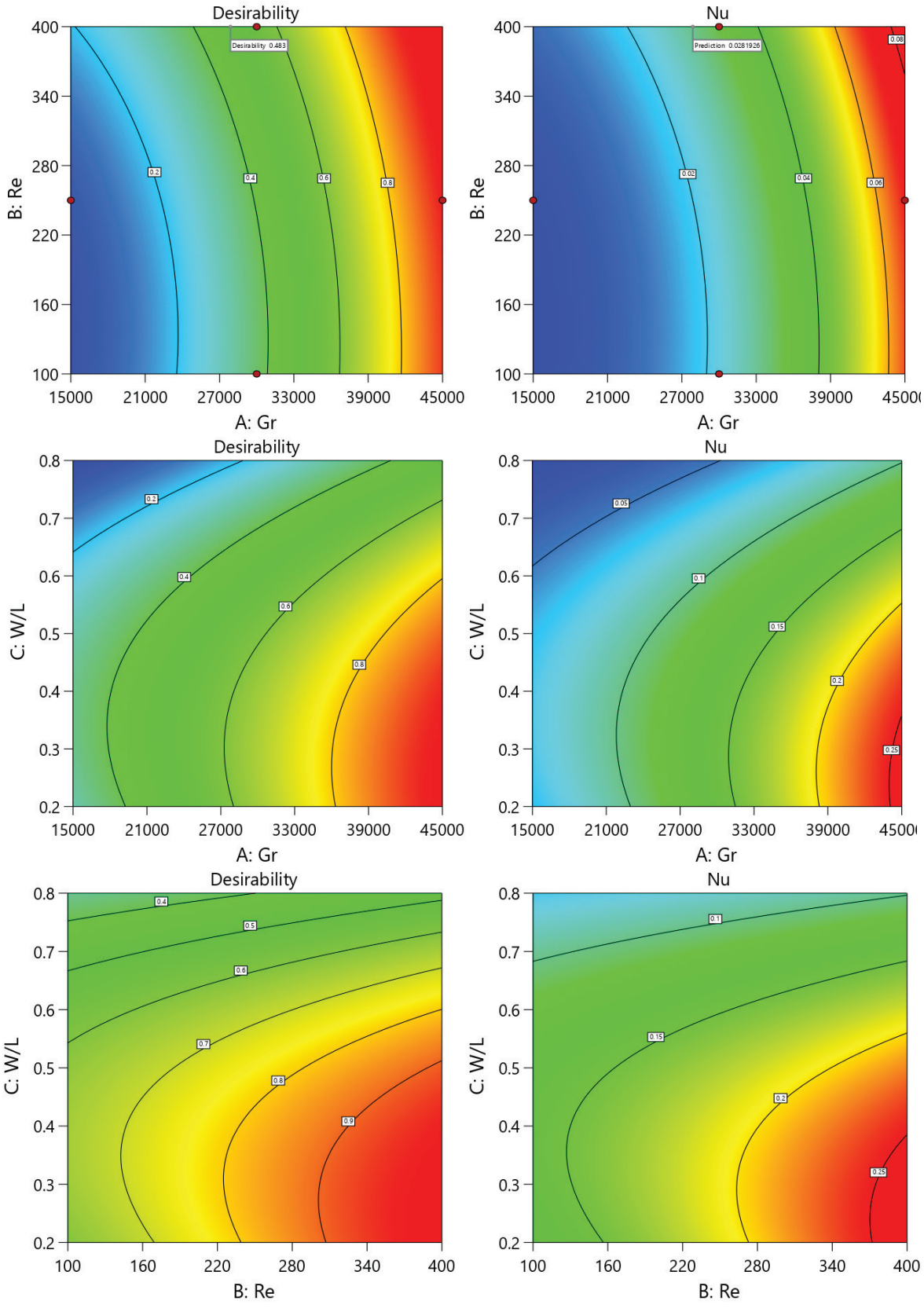

Figure 10. Validation of the predicted models.

CONCLUSION

The present research work used numerical methods to examine the convection process in a cavity with a lid-driven motion, which has two rectangular blocks within. To study the heat transfer in mixed convection with the variation of Grashof number. To study the heat transfer in mixed convection with the variation of Reynolds number. Optimization of obtained numerical results by using multi-objective optimization tool (Response Surface Methodology Approach). Following are the conclusions drawn:

1. The W/L ratio in the validation case is 0.25. In this case the walls of obstacles are kept at high temperatures whereas the boundary walls of the outer square cavity are at low temperature. However, the upper lid is in motion in positive x direction.
2. The streamlines form a vortex on the top whose size decreases as we move from left to right in case of Ri value 0.1. For Ri is equal to 1, another vortex besides the upper one is formed at the left corner.
3. The pattern of the vortex intensifies with the increase in Grashof and Reynolds numbers. It increases with the increase of the Grashof number. In the middle channel, there are not many formations of the vortices as there is less gap between the two obstacles.
4. The secondary vortex is formed due to the detached flow of the fluid. One vortex is due to forced convection which is due to the moving lid at the top and the other one is due to the natural convection at the lower end of the block.
5. As the Re is increased in all the cases, the intensity of the top vortex is increased due to the forced convection. With the decrease in the Grashof number from 10^5 to 15000, the second vortex completely disappears due to the decrease of the natural convection coefficient.
6. The motion of the particles occurs due to the cold flow and the hot fluid which is present at the bottom is pushed into the middle which helps to achieve the greater Grashof number due to unbalanced cohesive forces.
7. Nusselt numbers indicate that there is a minute reduction in the values. The Nusselt number values are high for Re = 500 for W/L equal to 0.2 and 0.8. And Nu value is high for Re = 250 for W/L = 0.2. Compared to all the orientation cases the highest Nu is in case of the closest arrangement of rectangular blocks that are for W/L = 0.2.
8. The R^2 values for the output variables $Nu_{horizontal}$ and $Nu_{vertical}$ are 0.96 and 0.94, respectively. The R^2 values for the projected models show a remarkable proximity to 1, indicating a significant degree of accuracy compared to the analytical outcomes. It has been noted that the effectiveness of the constructed prediction model is better when the values of comparative analysis and R^2 are low.

NOMENCLATURE

PBLHTES system	Packed bed Thermal energy storage system
EPCM	Encapsulated Phase Change Materials
TES	Thermal Energy Storage
npcm	Nano PCM
HTF	High Temperature Fluid
MWCNT	Multi Walled Carbon Nano Tubes
ρ_{eff}	Effective thermal conductivity of nano PCM
μ_{eff}	Effective viscosity of the nano PCM
β	Liquid Fraction
k_{eff}	Effective thermal conductivity of the nano PCM
Cp_{eff}	Effective specific heat of the nano PCM
u, v	Velocity of fluid in X and Y directions

AUTHORSHIP CONTRIBUTIONS

Authors equally contributed to this work.

DATA AVAILABILITY STATEMENT

The authors confirm that the data that supports the findings of this study are available within the article. Raw data that support the finding of this study are available from the corresponding author, upon reasonable request.

CONFLICT OF INTEREST

The authors declared no potential conflicts of interest with respect to the research, authorship, and/or publication of this article.

ETHICS

There are no ethical issues with the publication of this manuscript.

REFERENCES

[1] Bejan A. Convection Heat Transfer. New York: John Wiley & Sons; 2013. [CrossRef]

[2] Kandasamy R, Xiang-Qi W, Mujumdar AS. Transient cooling of electronics using phase change material (PCM)-based heat sinks. Appl Therm Eng 2008;28:1047−1057. [CrossRef]

[3] Papanicolaou E, Belessiotis V. Transient development of flow and temperature fields in an underground thermal storage tank under various charging modes. Solar Energy 2009;83:1161−1176. [CrossRef]

[4] Hamouche A, Bessaïh R. Mixed convection air cooling of protruding heat sources mounted in a horizontal channel. Int Comm Heat Mass Transf 2009;36:841−849. [CrossRef]

[5] Mathew VK, Hotta TK. Numerical investigation on optimal arrangement of IC chips mounted on a SMPS board cooled under mixed convection. Therm Sci Eng Prog 2018;7:221–229. [CrossRef]
[6] Zhou Y, Wang M, Wang M, Wang Y. Predictive accuracy of Boussinesq approximation in opposed mixed convection with a high-temperature heat source inside a building. Build Environ 2018;144:349–356. [CrossRef]
[7] Vera S, Rao J, Fazio P, Campo A. Mixed convective heat transfer through a horizontal opening in a full-scale, two-story test-hut. Appl Therm Eng 2014;64:499–507. [CrossRef]
[8] Selmi M, Al-Khawaja MJ, Marafia A. Validation of CFD simulation for flat plate solar energy collector. Renew Energy 2008;33:383–387. [CrossRef]
[9] Xiao C, Liao Q, Fu Q, Huang Y, Xia A, Chen H, et al. Numerical investigation of laminar mixed convection of microalgae slurry flowing in a solar collector. Appl Therm Eng 2020;175:115366. [CrossRef]
[10] Ghia UKNG, Ghia KN, Shin CT. High-Re solutions for incompressible flow using the Navier-Stokes equations and a multigrid method. J Comp Physics 1982;48:387–411. [CrossRef]
[11] Zheng GF, Ha MY, Yoon HS, Park YG. A numerical study on mixed convection in a lid-driven cavity with a circular cylinder. J Mech Sci Technol 2013;27:273–286. [CrossRef]
[12] Khaleel A, Gao S. CFD investigation of turbulent mixed convection heat transfer in a closed lid-driven cavity. Int J Civil Environ Eng 2015;9:1572–1577.
[13] Lee SC, Cha›o-Kuang C. Finite element solutions of laminar and turbulent mixed convection in a driven cavity. Int J Numer Methods Fluids 1996;23:47–64. [CrossRef]
[14] Mahapatra, Ray T, Pal D, Mondal S. Effects of buoyancy ratio on double-diffusive natural convection in a lid-driven cavity. Int J Heat Mass Transf 2013;57:771–785. [CrossRef]
[15] Roy S, Basak T. Finite element analysis of natural convection flows in a square cavity with non-uniformly heated wall (s). Int J Eng Sci 2005;43:668–680. [CrossRef]
[16] Gibanov NS, Sheremet MA, Oztop HF, Al-Salem K. Convective heat transfer in a lid-driven cavity with a heat-conducting solid backward step under the effect of buoyancy force. Int J Heat Mass Transf 2017;112:158–168. [CrossRef]
[17] Santos EDD, Petry AP, Rocha LAO, França FHR. Numerical study of forced convection lid-driven cavity flows using LES (Large Eddy Simulation). RCAAP 2013:5069.
[18] Yapici K, Obut S. Laminar mixed-convection heat transfer in a lid-driven cavity with modified heated wall. Heat Transf Eng 2015;36:303–314. [CrossRef]
[19] Cheng CH, Chin-Lung C. Buoyancy-induced periodic flow and heat transfer in lid-driven cavities with different cross-sectional shapes. Int Comm Heat Mass Transf 2005;32:483–490. [CrossRef]
[20] Idris MS, Irwan MAM, Ammar NMM. Steady state vortex structure of lid driven flow inside shallow semi-ellipse cavity. J Mech Eng Sci 2012;2:206–216. [CrossRef]
[21] Shah SS, Haq RU, Al-Kouz W. Mixed convection analysis in a split lid-driven trapezoidal cavity having elliptic shaped obstacle. Int Comm Heat Mass Transf 2021;126:105448. [CrossRef]
[22] Haq RU, Soomro FA, Wang X, Tlili I. Partially heated lid-driven flow in a hexagonal cavity with inner circular obstacle via fem. Int Comm Heat Mass Transf 2020;117:104732. [CrossRef]
[23] Xiong PY, Hamid A, Iqbal K, Irfan M, Khan M. Numerical simulation of mixed convection flow and heat transfer in the lid-driven triangular cavity with different obstacle configurations. Int Comm Heat Mass Transf 2021;123:105202. [CrossRef]
[24] Yasin A, Ullah N, Nadeem S, Ghazwani HA. Numerical simulation for mixed convection in a parallelogram enclosure: Magnetohydrodynamic (MHD) and moving wall-undulation effects. Int Comm Heat Mass Transf 2022;135:106066. [CrossRef]
[25] Jiang X, Hatami M, Abderrahmane A, Younis O, Makhdoum BM, Guedri K. Mixed convection heat transfer and entropy generation of MHD hybrid nanofluid in a cubic porous cavity with wavy wall and rotating cylinders. Appl Therm Eng 2023;226:120302. [CrossRef]
[26] Khan NZ, Mahmood R, Bilal S, Akgül A, Abdullaev S, Mahmoud EE, et al. Mixed convective thermal transport in a lid-driven square enclosure with square obstacle. Alexandria Eng J 2023;64:981–998. [CrossRef]
[27] Ali MM, Akhter R, Alim MA. Magneto-mixed convection in a lid driven partially heated cavity equipped with nanofluid and rotating flat plate. Alexandria Eng J 2022;61:257–278. [CrossRef]
[28] Yaseen DT, Salih SM, Ismael MA. Effect of the lid-driven on mixed convection in an open flexible wall cavity with a partially heated bottom wall. Int J Therm Sci 2023;188:108213. [CrossRef]
[29] Alsabery AI, Tayebi T, Kadhim HT, Ghalambaz M, Hashim I, Chamkha AJ. Impact of two-phase hybrid nanofluid approach on mixed convection inside wavy lid-driven cavity having localized solid block. J Adv Res 2021;30:63–74. [CrossRef]
[30] Kalogirou SA. Applications of artificial neural networks in energy systems. Energy Convers Manag 1999;40:1073–1087. [CrossRef]
[31] Belanger S, Gosselin L. Utilization of artificial neural networks in the context of materials selection for thermofluid design. Numer Heat Transf Part A Appl 2009;55:825–844. [CrossRef]

[32] Deng S, Hwang Y. Solving the temperature distribution field in nonlinear heat conduction problems using the Hopfield neural network. Numer Heat Transf Part B Fundamentals 2007;51:375–389. [CrossRef]
[33] Mahmoud MA, Ben-Nakhi AE. Neural networks analysis of free laminar convection heat transfer in a partitioned enclosure. Comm Nonlinear Sci Numer Sim 2007;12:1265–1276. [CrossRef]
[34] Selimefendigil F, Öztop HF. Fuzzy-based estimation of mixed convection heat transfer in a square cavity in the presence of an adiabatic inclined fin. Int Comm Heat Mass Transf 2012;39:1639–1646. [CrossRef]
[35] Aminossadati SM, Kargar A, Ghasemi B. Adaptive network-based fuzzy inference system analysis of mixed convection in a two-sided lid-driven cavity filled with a nanofluid. Int J Therm Sci 2012;52:102–111. [CrossRef]
[36] Filali A, Khezzar L, Semmari H, Matar O. Application of artificial neural network for mixed convection in a square lid-driven cavity with double vertical or horizontal oriented rectangular blocks. Int Comm Heat Mass Transf 2021;129:105644. [CrossRef]
[37] Hosseinzadeh K, Roshani M, Attar MA, Ganji DD, Shafii MB. Heat transfer study and optimization of nanofluid triangular cavity with a pentagonal barrier by finite element approach and RSM. Heliyon 2023;9:e20193. [CrossRef]
[38] Kolsi L, Öztop HF, Abu-Hamdeh N, Naceur BM, Ben Assia H. Effects of moving lid direction on mixed convection and entropy generation in a cubical cavity with longitudinal triangular fin insertion. Int J Numer Meth Heat Fluid Flow 2017;27:839–860. [CrossRef]
[39] Ching YC, Öztop HF, Rahman MM, Islam MR, Ahsan A. Finite element simulation of mixed convection heat and mass transfer in a right triangular enclosure. Int Comm Heat Mass Transf 2012;39:689–696. [CrossRef]
[40] Saha G, Al-Waaly AA, Paul MC, Saha SC. Heat transfer in cavities: configurative systematic review. Energies 2023;16:2338. [CrossRef]
[41] Uddin MB, Rahman MM, Khan MAH, Ibrahim TA. Effect of buoyancy ratio on unsteady thermosolutal combined convection in a lid driven trapezoidal enclosure in the presence of magnetic field. Comp Fluids 2015;114:284–296. [CrossRef]
[42] Sivasubramanian M, Kanna PR, Rajesh S, Uthayakumar M. Experimental investigation on heat transfer enhancement from a channel with square blocks and identification of most influencing parameters using Taguchi approach. Proc Inst Mech Eng Part C J Mech Eng Sci 2016;230:3253–3266. [CrossRef]
[43] Teja PNS, Gugulothu SK, Reddy PDS, Deepanraj B. Numerical investigation of nanoparticles dispersion on forced/mixed convective flows and heat transfer in a lid-driven stepped cavity configurations. Proc Inst Mech Eng Part E J Proc Mech Eng 2022;239:09544089221127617. [CrossRef]
[44] Ilicak M, Ecder A, Turan E. Operator splitting techniques for the numerical analysis of natural convection heat transfer. Comp Math 2007;84:783–793. [CrossRef]
[45] Addini MM, Nassab SA. Combined mixed convection and radiation heat transfer in an obstacle wall mounted lid-driven cavity. Int J Nonlinear Sci Numer Sim 2016;17:277–289. [CrossRef]
[46] Rais AI, Mahmud MJ, Hossain MR, Saha S. Influence of heat generation/absorption on mixed convective flow in a lid-driven chamber with isothermal rotating cylinder. Ann Nuc Energy 2023;182:109596. [CrossRef]
[47] Nowak AJ, Bialecki RA. Special issue: Selected papers from the International Scientific Conference on Numerical Heat Transfer 2005. Int J Numer Meth Heat Fluid Flow 2008;18:13418caa.001.
[48] Selimefendigil F. Natural convection in a trapezoidal cavity with an inner conductive object of different shapes and filled with nanofluids of different nanoparticle shapes. Iranian J Sci Technol Transact Mech Eng 2018;42:169–184. [CrossRef]
[49] Sivasankaran S, Cheong HT, Bhuvaneswari M, Ganesan P. Effect of moving wall direction on mixed convection in an inclined lid-driven square cavity with sinusoidal heating. Numer Heat Transf Part A Appl 2016;69:630–642. [CrossRef]
[50] Bockting-Conrad S, Terwilliger P. The algebra Uq (sl2) in disguise. Linear Algebra Appl 2014;459:548–585. [CrossRef]
[51] Mandal DK, Biswas N, Manna NK, Gorla RSR, Chamkha AJ. Hybrid nanofluid magnetohydrodynamic mixed convection in a novel W-shaped porous system. Int J Numer Meth Heat Fluid Flow 2023;33:510–544. [CrossRef]
[52] Mandal SK, Deb A, Sen D. Mixed convective heat transfer with surface radiation in a rectangular channel with heat sources in presence of heat spreader. Therm Sci Eng Prog 2019;14:100423. [CrossRef]
[53] Khoei AR, Mousavi SM, Hosseini N. Modeling density-driven flow and solute transport in heterogeneous reservoirs with micro/macro fractures. Adv Water Res 2023;182:104571. [CrossRef]
[54] Khoei AR, Saeedmonir S, Hosseini N, Mousavi SM. An X–FEM technique for numerical simulation of variable-density flow in fractured porous media. MethodsX 2023;10:102137. [CrossRef]
[55] Zare S, Makki M, Rasooli M, Alavi HS, Tavakolpour-Saleh AR. Assessment of a diaphragm thermoacoustic Stirling engine using the energy standpoint and genetic algorithm. Int J Energy Environ Eng 2023;14:743–755. [CrossRef]

[56] Amini H, Mehrizi-Sani A, Liu CC. Substation cyberattack detection and mitigation in a high-noise environment. Proceedings of 2024 IEEE Power & Energy Society Innovative Smart Grid Technologies Conference (ISGT); 2024. pp. 1–5. [CrossRef]

[57] Roy PP, Chowdhury S, Raj MH, Islam MQ, Saha S. Forced, natural and mixed convection of Non-Newtonian fluid flows in a square chamber with moving lid and discrete bottom heating. Results Eng 2024;17:100939. [CrossRef]

[58] Morshed KN, Sharif MA, Islam AW. Laminar mixed convection in a lid-driven square cavity with two isothermally heated square internal blockages. Chem Eng Comm 2015;20:1176–1190. [CrossRef]

[59] Kumar PP, Pendyala S, Gugulothu SK. Influences of iso-amyl nitrate oxygenated additive on mahua methyl ester/diesel blends thermal stability and crdi engine performance characteristics. J Therm Eng 2024;10:447–456. [CrossRef]

[60] Gugulothu SK. Enhancement of household refrigerator energy efficiency by studying the effect of refrigerant charge and capillary tube length. J Therm Eng 2021;7:1121–1129. [CrossRef]

[61] Shaik R, Punna E, Gugulothu S. Numerical investigation on comparative performance assessment of solar air heater with different artificial roughness elements in a triangular duct. J Therm Eng 2025;11:49–61. [CrossRef]